Supporting Information

Realizing avalanche criticality in neuromorphic networks on 2D hBN platform

Ankit Rao[1], Sooraj Sanjay[1], Vivek Dey[1], Majid Ahmadi[2], Pramod Yadav[1], Anirudh Venugopalrao[1], Navakanta Bhat[1], Bart Kooi[2,3], Srinivasan Raghavan[1], Pavan Nukala[1].

[1]Centre for Nano Science and Engineering, Indian Institute of Science, Bengaluru 560012, [2]Zernike Institute for Advanced Materials, University of Groningen, Groningen, the Netherlands, [3]CogniGron center, University of Groningen, Groningen, 9747 AG, The Netherlands.

This file includes:

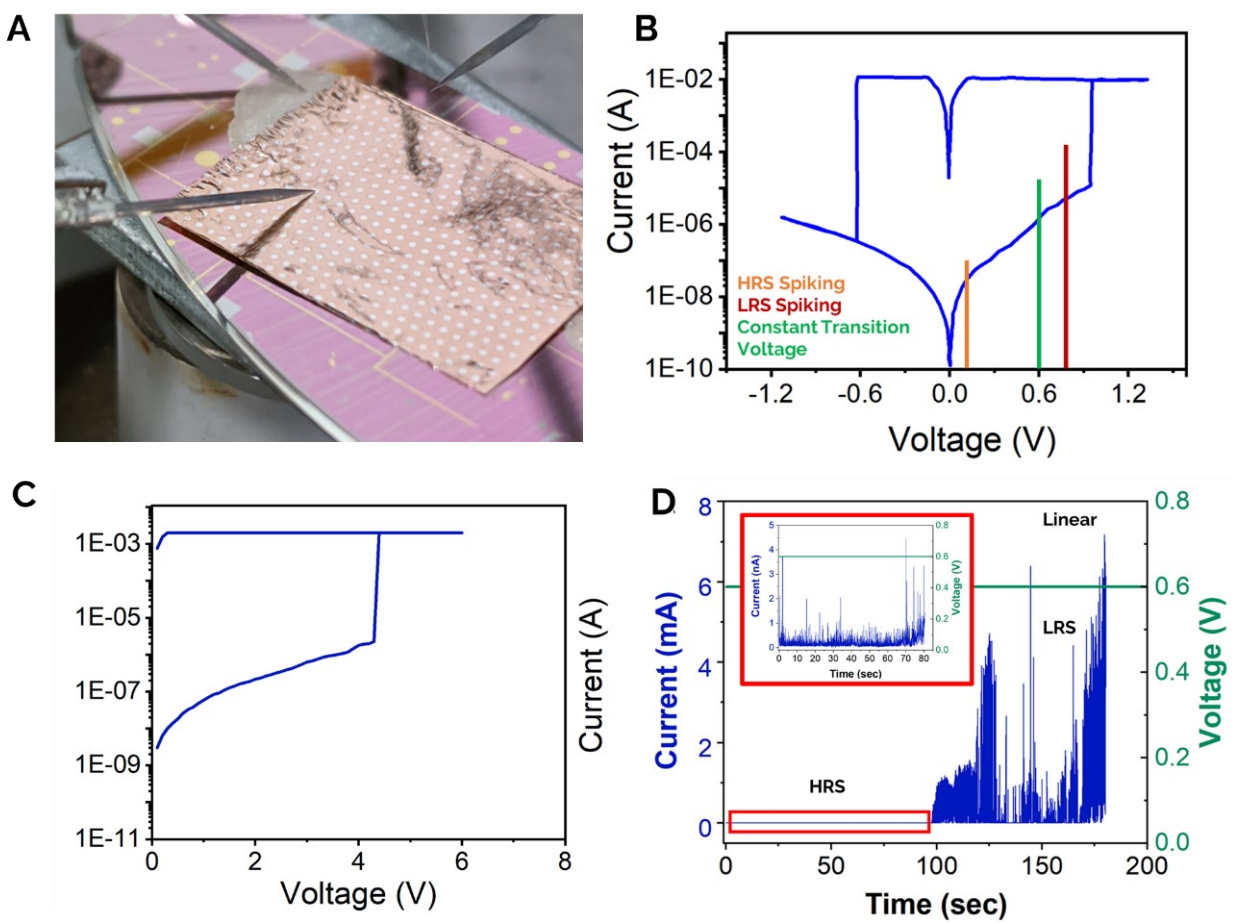

Figure S1. A) Large Area Ag-hBN-Cu device. B) Resistive switching behavior observed in the device at SET voltage (0.9V) and RESET voltage (0.6V). C) Electroforming process for the Ag-hBN device with forming voltage (V_f) of ~4V. D) Current-time plot in linear scale at a constant voltage of 0.6V. The temporal behavior of device exhibiting transition from HRS to LRS due to transport of ions under constant electric field. (Inset) The HRS pattern observed scaled to the current levels of the device in nA.

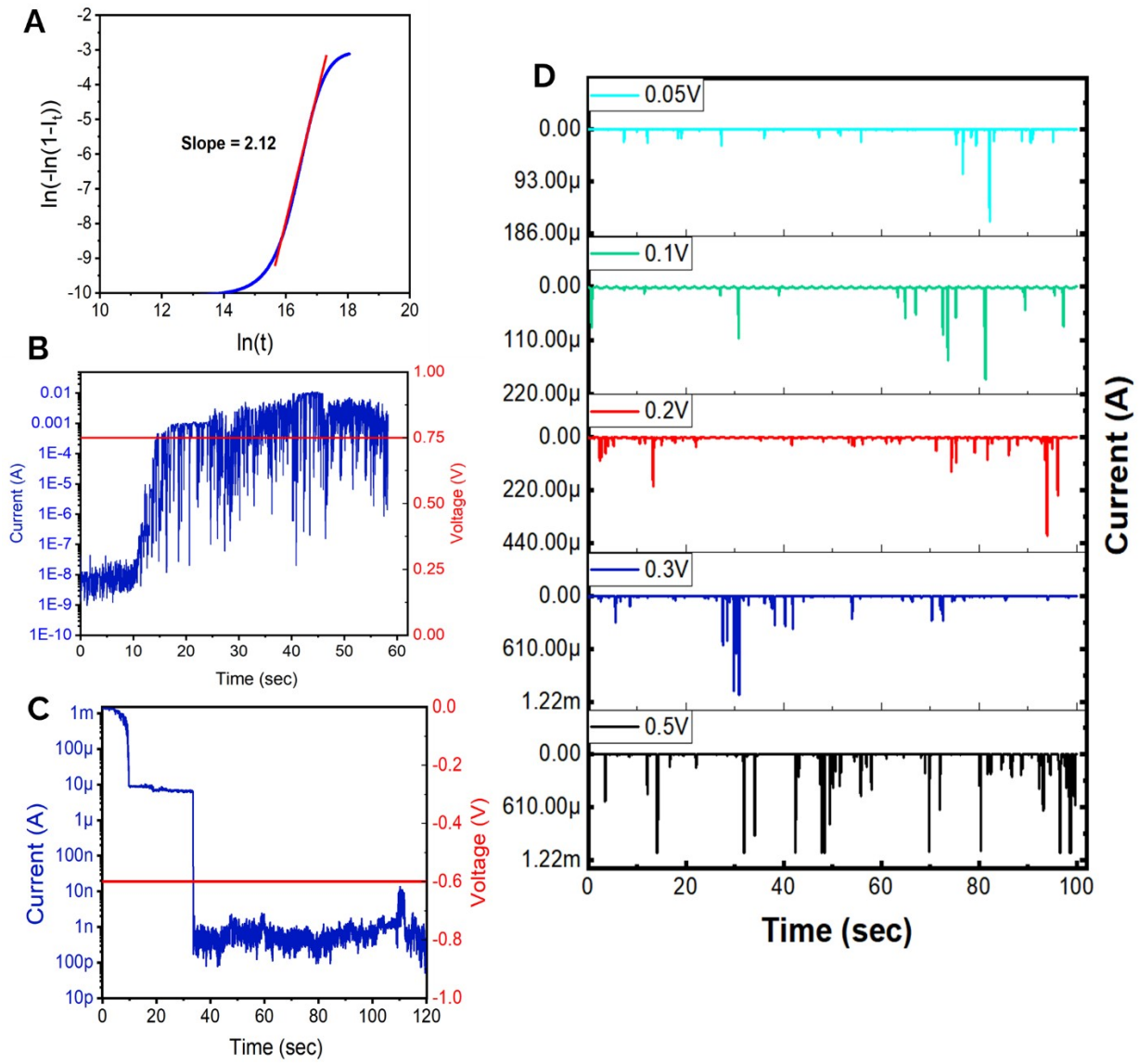

Figure S2. A) Avrami exponent determination from the ln(-ln(1-x) vs ln(t) curve. B) Time series plot current at 0.75V indicating faster transition due to increased voltage. C) Time series plot of current under constant negative bias (-0.6V) resulting in filamentary breakage and reversal phenomenon. D) Rate coding. Controlling spiking rate as a function of input voltage. Spiking rate can be used to encode information for a specific input voltage.

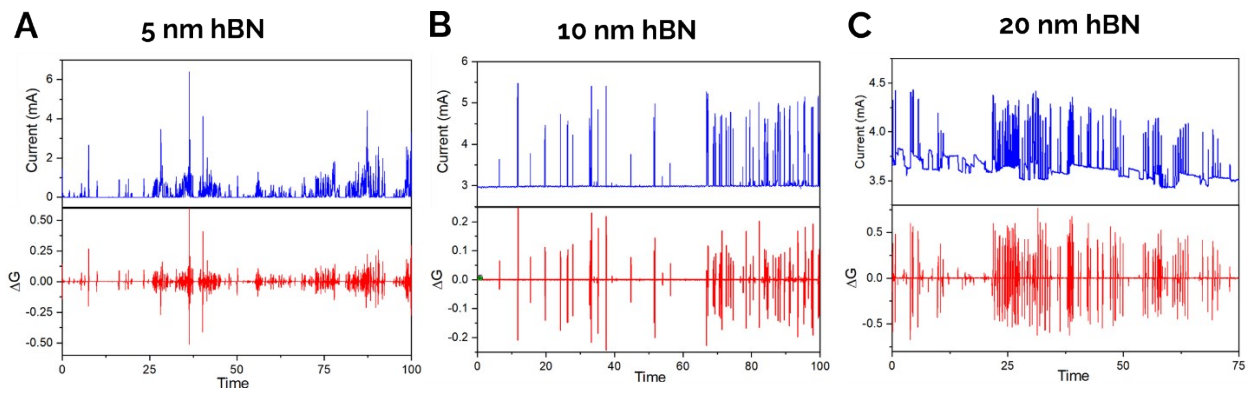

Figure S3 – A) to C) Current spiking data for devices with hBN thicknesses of 5nm, 10nm and 20nm respectively along with ΔG.

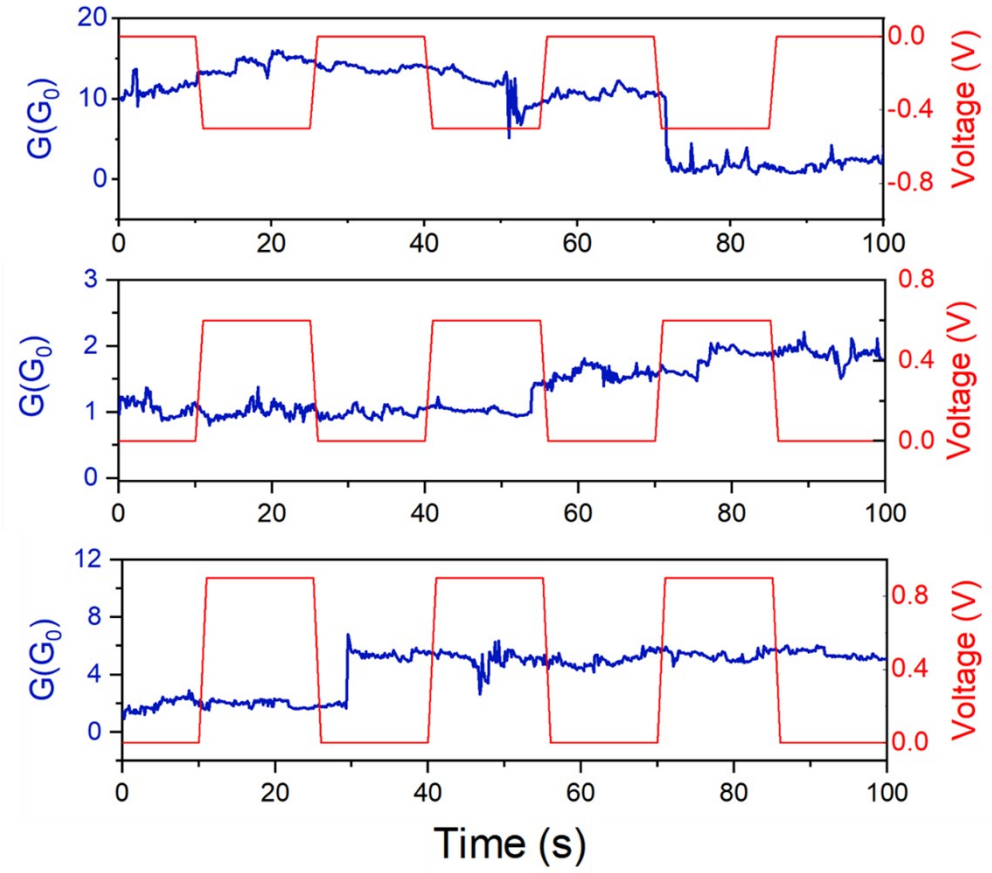

Figure S4. Diffusion based self-stabilizing behavior under application of long-range pulsed stimulus. (Top Panel) Under negative voltage stimulus (-0.6V), when the system is at higher conductance levels, the filaments tend to break and return to lower conductance levels. (Middle Panel) Pulsing at a voltage (0.6V) lower than the SET voltage allows the system to stay in a stable configuration with small temporal change in conductance. (Bottom Panel) Under pulsing at voltage (0.8V) closer to SET point, the system conductance increases due to diffusion under application of higher fields.

Long Range Pulsed Stimulus

When negative voltage pulses in LRS state are applied (-0.6V), the system tends to switch from a high conductance level and the return to low conductance level as the filaments tend to break. When the device is in HRS state, the pulsing is applied at a voltage (0.6V) lower than the SET voltage which allows the system to stay in a stable configuration as small temporal changes in conductance are observed. Under pulsing at voltage (0.8V) closer to SET point, the system conductance increases due to diffusion under application of higher fields.

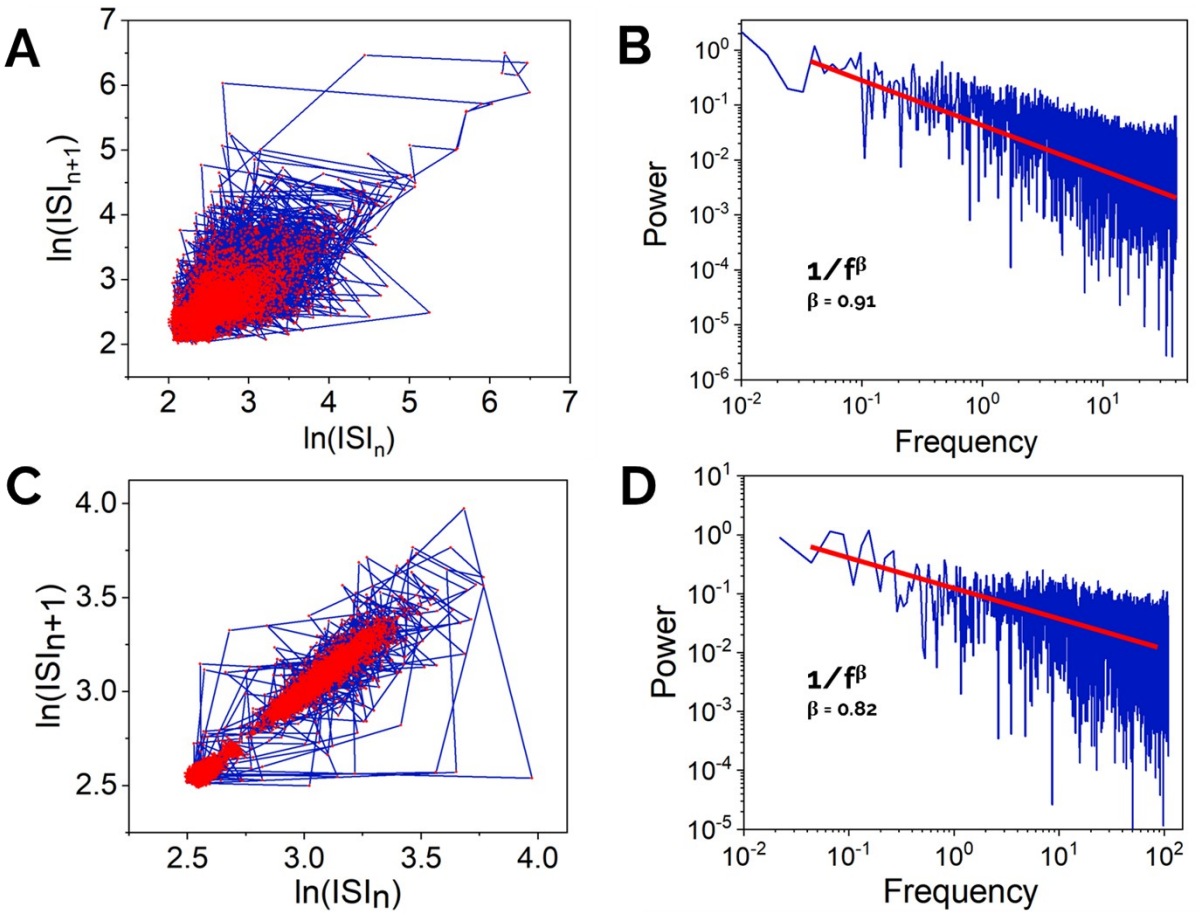

Figure S5. (A and C) Correlation between successive inter-spike intervals (ISI_n) for HRS and LRS cases. (B and D) Power Distribution (A^2/Hz) as a function of frequency (Hz) plot for determination of 1/f noise and β exponent value for HRS and LRS.

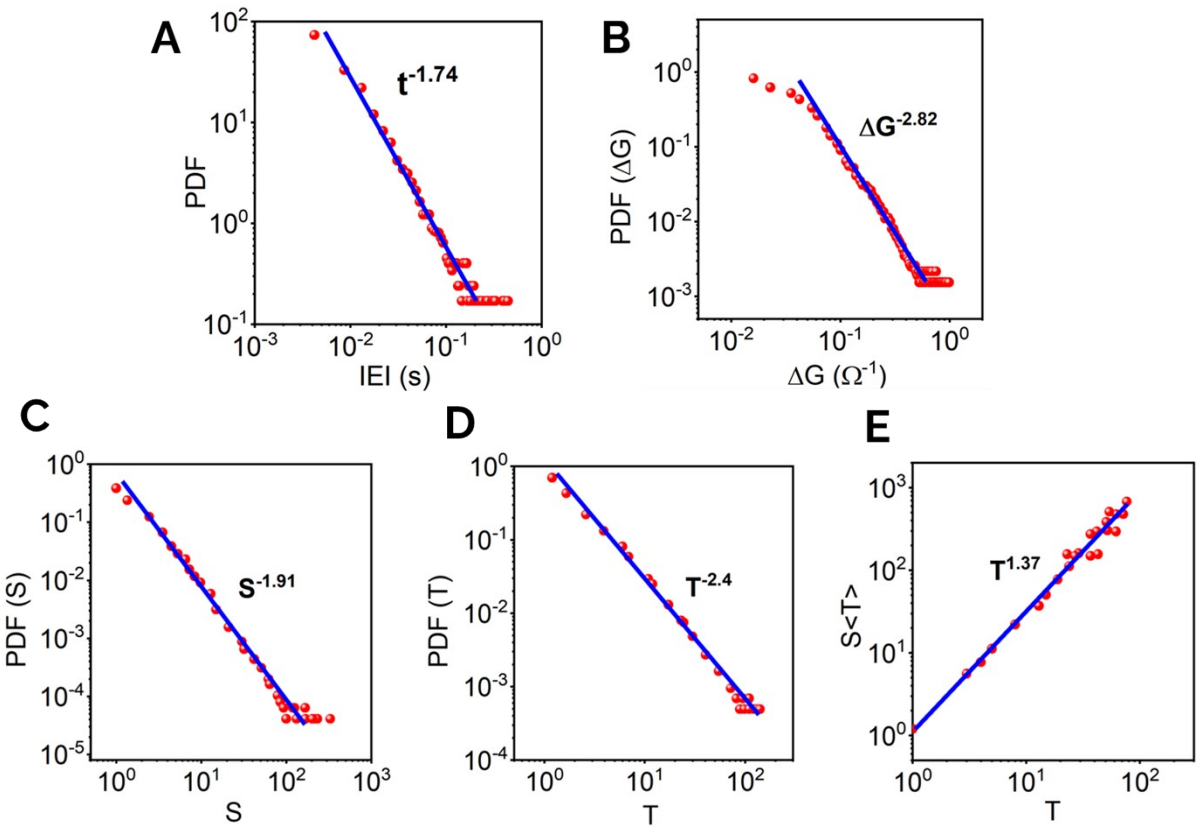

Figure S6. Statistics of Avalanche behavior for 1 ms sampling rate in LRS (A and B) Probability density function of IEI and Change in conductance. (C, D and E) Probability density functions of size of an avalanche (S), duration of an avalanche (T) and average avalanche size per unit time bin <S>(T) respectively. All the distributions exhibit power laws with exponents similar to 10 ms sampling.

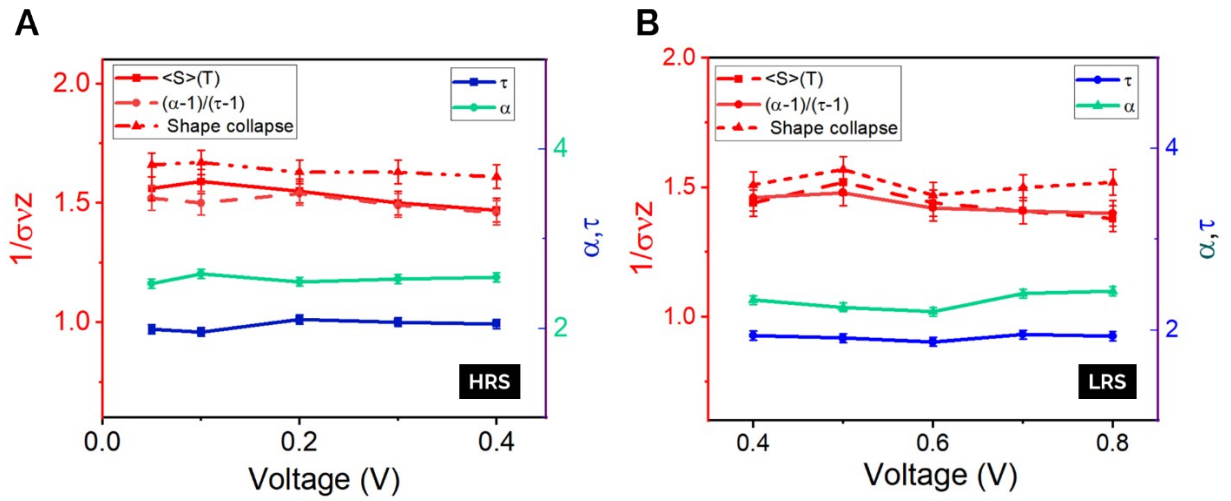

Figure S7. Variation of estimations of 1/σνz as a function of voltage from <S>(T) vs T, (α-1)/(τ-1) and shape collapse analysis. Trend of critical exponents (α, τ) as a function of voltage for HRS (A) and LRS (B).

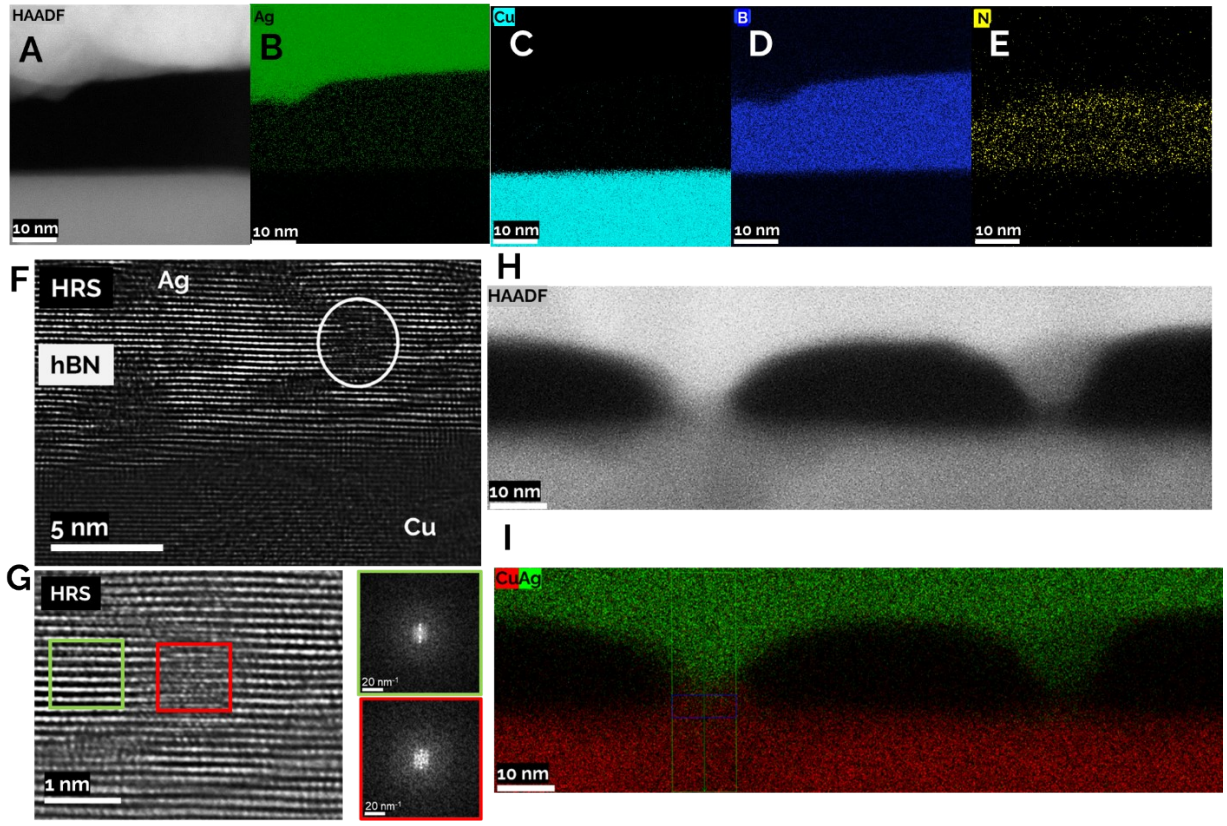

Figure S8. (A to E) HAADF-STEM EDS mapping of Ag-hBN-Cu stack in the HRS state. F) HRTEM image of the cross section from same sample after 10 switching cycles and rested in HRS state. G) Magnified area from F) (white region) which suggests the presence of an intercalated planar cluster of Ag between two hBN layers. H) The Fast Fourier Transform (FFT) of the regions pristine (green) and defective (red) from G) confirms change in the crystallinity of the structure due to Ag intercalation. I, J) HAADF-STEM (I) EDS (J) mapping of the Ag-hBN-Cu in the LRS state showing formation of Ag filaments.

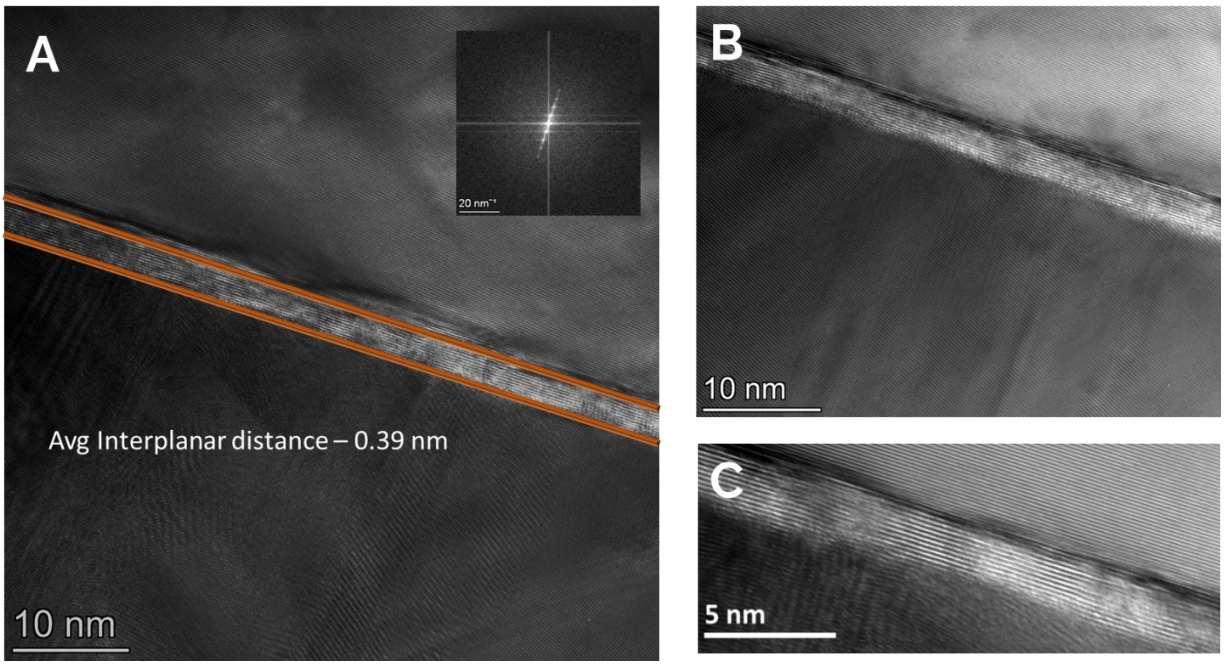

Figure S9. HRTEM Imaging for different field of views A) 100x100 nm, B) 50x50 nm and C) 15x15nm.

Table S1. Critical Exponents

	ΔG	IEI	τ	α	1/σνz
HRS	2.59±0.05	1.54±0.05	1.98±0.1	2.61±0.1	1.59±0.03
LRS	2.87±0.05	1.72±0.05	1.93±0.1	2.43±0.1	1.38±0.03
Nanoparticle Network[1]	2.59	1.93	2.05±0.1	2.66±0.1	1.55±0.03
Nanowire Network[2]	-	-	2±0.1	2.3±0.1	1.3±0.03
Rat cortices[3]	-	-	1.74	1.96	1.22
Neuronal cortices[4]	-	-	1.69	1.92	1.56

(*Error Analysis - This standard deviation is used as a measure of the error of the exponent of the original fit, and is estimated from the routines presented in Ref 44)

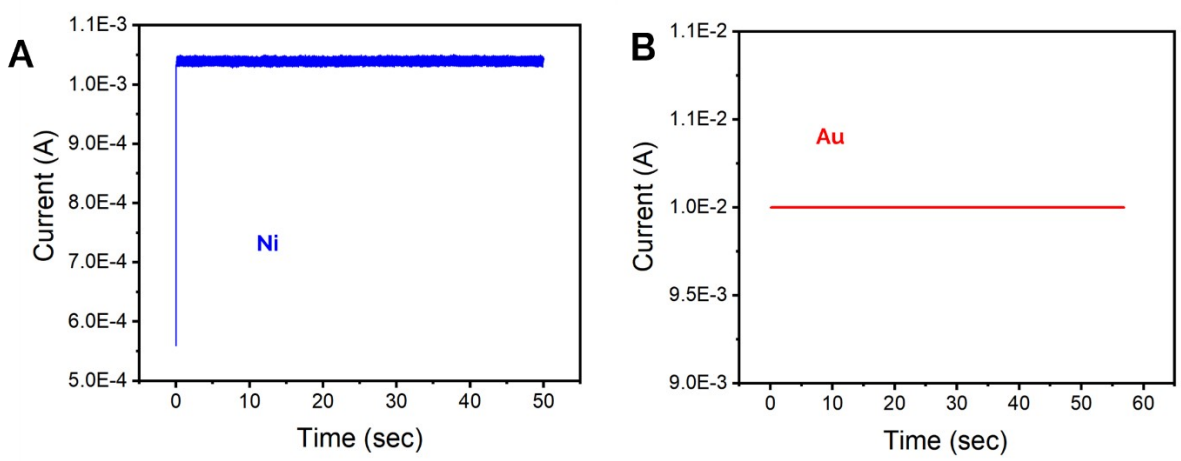

Figure S10. A) Ni and B) Au as the top electrode. No spiking behavior is observed with Ni and Au as the top electrode.

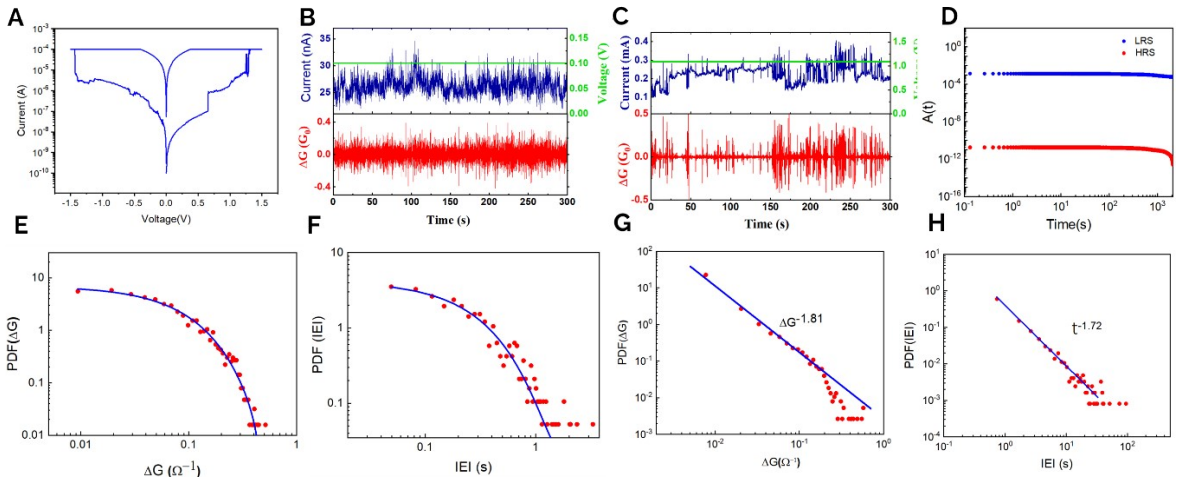

Figure S11. A) Resistive switching behaviour in Ag-Yttria Stabilized Zirconia (YSZ)-TiN device. B) Current voltage sampling as a function of time for the device in HRS shows non-critical spiking which is random noise behaviour. C) In LRS the device shown has similar behaviour to Ag-hBN system. D) Autocorrelation function (ACF) show no correlation in HRS (ACF~0) whereas there is power law dependence in LRS. E) and F) The probability distribution function (PDF) of ΔG and IEI for the device in HRS show exponential behaviour, thus they do not follow power law. G) and H) PDFs of ΔG and IEI of the device in LRS show power law dependence.

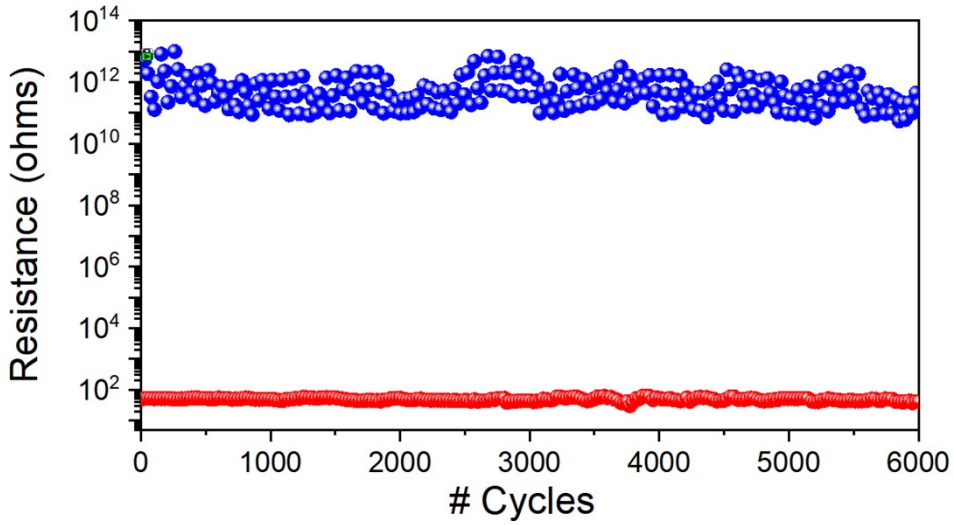

Figure S12 - hBN RRAM endurance characteristics. Even after 6000 cycles this device functions very well, and the underlying network behavior also sustains. As an outlook, it is important to understand fatigue of network behavior upon further cycling, and this is different (and will have stricter constraints) than the fatigue of the device as a CBRAM for memory applications.

References

(1) Pike, M. D.; Bose, S. K.; Mallinson, J. B.; Acharya, S. K.; Shirai, S.; Galli, E.; Weddell, S. J.; Bones, P. J.; Arnold, M. D.; Brown, S. A. Atomic Scale Dynamics Drive Brain-like Avalanches in Percolating Nanostructured Networks. *Nano Lett.* **2020**, *20* (5), 3935–3942. https://doi.org/10.1021/acs.nanolett.0c01096.

(2) Hochstetter, J.; Zhu, R.; Loeffler, A.; Diaz-Alvarez, A.; Nakayama, T.; Kuncic, Z. Avalanches and Edge-of-Chaos Learning in Neuromorphic Nanowire Networks. *Nat. Commun.* **2021**, *12* (1). https://doi.org/10.1038/s41467-021-24260-z.

(3) Friedman, N.; Ito, S.; Brinkman, B. A. W.; Shimono, M.; DeVille, R. E. L.; Dahmen, K. A.; Beggs, J. M.; Butler, T. C. Universal Critical Dynamics in High Resolution Neuronal Avalanche Data. *Phys. Rev. Lett.* **2012**, *108* (20), 208102. https://doi.org/10.1103/PhysRevLett.108.208102.

(4) Ponce-Alvarez, A.; Jouary, A.; Privat, M.; Deco, G.; Sumbre, G. Whole-Brain Neuronal Activity Displays Crackling Noise Dynamics. *Neuron* **2018**, *100* (6), 1446-1459.e6. https://doi.org/10.1016/j.neuron.2018.10.045.